REPORT

Ratiometric imaging of gastrodermal lipid bodies in coral–dinoflagellate endosymbiosis

Y.-J. Luo · L.-H. Wang · W.-N. U. Chen · S.-E. Peng ·
J. T.-C. Tzen · Y.-Y. Hsiao · H.-J. Huang ·
L.-S. Fang · C.-S. Chen

Abstract Cnidaria–dinoflagellate endosymbiosis is the phenomenon of autotrophic symbionts living inside the gastrodermal cells of their animal hosts. The molecular mechanism that regulates this association remains unclear. Using quantitative microscopy, we now provide evidence that the dynamic lipid changes in gastrodermal "lipid bodies" (LBs) reflect the symbiotic status of the host cell and its symbiont in the hermatypic coral *Euphyllia glabrescens*. By dual-emission ratiometric imaging with a solvatochromic fluorescent probe, Nile red (9-diethyl-amino-5H-benzo[α]phenoxazine-5-one), we showed that the in situ distribution of polar versus neutral lipids in LBs in living gastrodermal cells and symbionts can be analyzed. The ratio of Nile red fluorescence at red (R) versus green (G) wavelength region (i.e., R/G ratio) correlated with the relative molar ratio of polar (P) versus neutral (NP) lipids (i.e., P/NP ratio). The R/G ratio in host LBs increased after bleaching, indicating a decrease in neutral lipid accumulation in gastrodermal cells. On the other hand, neutral lipid accumulation inside the symbiont LBs resulted in gradual decreases of the R/G ratio as a result of bleaching. In comparison with the bleaching event, there was no relative lipid concentration change in host LBs under continual light or dark treatments as shown by insignificant R/G ratio shift. Patterns of R/G ratio shift in symbiont LBs were also different between corals undergoing bleaching and continual light/dark treatment. In the latter, there was little lipid accumulation in symbionts, with no resulting R/G ratio decrease. These results, demonstrating that the symbiotic status positively correlated with morphological and compositional changes of lipid bodies, not only highlight the pivotal role of LBs, but also implicate an involvement of lipid trafficking in regulating the endosymbiosis.

Keywords Coral bleaching · Nile red ·
Membrane trafficking · Lipid droplets · *Symbiodinium*

Communicated by Biology Editor Dr. Ruth Gates

Y.-J.Luo · L.-H.Wang · S.-E.Peng · Y.-Y.Hsiao · H.-J.Huang ·
C.-S.Chen (✉)
Institute of Marine Biotechnology, National Dong Hwa
University, Taiwan Coral Research Center, National Museum of
Marine Biology and Aquarium, 2 Houwan Road, Checheng,
Pingtung 944, Taiwan, ROC
e-mail: cchen@nmmba.gov.tw

W.-N.U. Chen
Department of Biological Science and Technology,
I-Sou University, Kaohsiung, Taiwan, ROC

J. T.-C.Tzen
Graduate Institute of Biotechnology,
National Chung Hsing University, Taichung, Taiwan, ROC

L.-S.Fang
Cheng Shiu University, Kaohsiung, Taiwan, ROC

Introduction

The mechanisms of cellular and molecular regulation of Cnidarian–dinoflagellate endosymbiosis remain unclear after decades of investigation (Muscatine 1967; Muscatine et al. 2005). The basic characteristic of this mutualistic association between animals (i.e., Cnidaria, such as corals, sea anemones, and jellyfishes) and their intracellular microalgal symbionts (i.e., the dinoflagellate or *Symbiodinium* sp.) is that there is transport of photosynthetic products from the symbionts to the gastrodermal cells of the host animals. Under normal conditions, the cell–cell transport of photosynthates is regulated, resulting in an endosymbiotic association that is beneficial for both the host cell and the

symbiont (Muscatine 1967; Wang and Douglas 1997). Using radioactive fatty acids and lipids, D'Elia and colleagues showed that, the endosymbiotic relationship between host cells and symbionts could be clearly demonstrated by lipid exportation and deposition in animal cells (D'Elia 1977; D'Elia et al. 1983). During endosymbiosis, $\sim 60\%$ of lipids generated inside the symbiont was exported into their host gastrodermal cells (Trench 1971; Wang and Douglas 1997; Biel et al. 2007). This lipid exportation was significantly abolished in *Symbiodinium* sp. freely cultured outside host animals. The morphological evidence of this lipid translocation was the formation of large host "lipid droplets" or "lipid bodies" (LBs) outside the symbiosome, which were first identified by Patton and Burris (1983) and later by others (Kellogg and Patton 1983; Battey and Patton 1984). The large LBs are phase-contrast positive within the host cell cytoplasm and thus can be easily identified by light microscopy. However, the structural and compositional characteristics of LBs and their direct functional role during endosymbiosis remain unclear.

LB formation and its role in lipid trafficking have been extensively examined in mammalian cells during the past 5 years (for a review see Martin and Parton 2006). Here, lipid bodies are pivotal cellular organelles with specific structural and functional characteristics. Structurally, they consist of a core of neutral lipids, predominantly triacylglycerols or cholesteryl esters that are surrounded by a monolayer of phospholipids and associated proteins (Martin and Parton 2005). Functionally, although LBs were originally recognized as depots for lipid storage, they are now regarded as a complex and dynamic organelle (Martin and Parton 2006) involved in membrane trafficking (Liu et al. 2004), cell signaling (Umlauf et al. 2004), lipid metabolism (Coleman and Lee 2004; Duncan et al. 2007), cholesterol homeostasis (Maxfield and Tabas 2005), and visual chromophore regeneration (Imanishi et al. 2004). In the present study, we identified the LBs formed during coral–dinoflagellate symbiotic association, and hypothesized that the LBs in the host gastrodermal cells are unique organelles whose dynamic changes in lipid compositions reflect the endosymbiotic status. The specific aims of the present study are to test this hypothesis by developing a method of live cell ratiometric imaging in order to examine lipid compositional changes of LBs in situ and to provide critical insight into the role of LBs during endosymbiosis.

Materials and methods

Reagents, culture medium, and filtered seawater

Iscove's Modified Dulbecco's Medium (IMDM, Gibco) with NaHCO$_3$ was purchased from Invitrogen Corporation (Carlsbad, CA, USA). IMDM solution for treating cells was prepared by adding 10% Fetal Bovine Serum plus antibiotics (Streptomycin, 100 µg ml^{-1}; Penicillin, 100 units ml^{-1}). All seawater used for the experiment was prepared by filtering through a VacuCap 90 filter unit (0.2 µm, Gelman Laboratory, Ann Arbor, MI, USA). Artificial seawater (ASW) was prepared as 420 mM NaCl, 26 mM MgSO$_4$, 23 mM MgCl$_2$, 9 mM KCl, 9 mM CaCl$_2$, 2 mM NaHCO$_3$, 10 mM Hepes, pH 8.2. The osmolarity of all solutions for treating cells was measured using a Micro-osmometer (Advanced Instruments, Inc., Norwood, MA, USA), and was adjusted to 1,000 mOs by adding NaCl. All chemicals were of analytical grade.

Coral collection, maintenance, and preparation of amputated tentacles

Coral colonies of *Euphyllia glabrescens* (7.2–35.8 cm in diameter) were collected by SCUBA divers from the inlet of the Third Nuclear Power Plant (21° 57.376′N, 120° 45.291′E) at a depth of 3–8 m in Nanwan Bay, Taiwan. Collected colonies were placed in an upright position in a 4-tone outdoor tank with flow-through seawater (at an exchange rate of ~ 80 l/h), a natural photoperiod and additional gas pumping in the husbandry center of the National Museum of Marine Biology and Aquarium (NMMBA). A microprocessor-controlled cooler was linked to the tank and the temperature was maintained at 25°C. Amputated tentacles were obtained from the polyps of the *E. glabrescens* colony using curved surgical scissors. The tentacles were then transferred to the lab and washed with filtered seawater (FSW) for further use.

Artificial manipulation of bleaching and continual light/dark treatment of *E. glabrescens*

To artificially induce coral bleaching, colonies of *E. glabrescens* were exposed to elevated (i.e., heat stress) temperatures in a 38-l plastic tank (58 × 39 × 18 cm, seawater height ~ 17 cm) placed indoors (background illumination of about 1 µmole m^{-2} s^{-1}). The shift in temperature to induce coral bleaching is shown in Fig. 1. Seawater was internally circulated using a submersible pump (22 W, 1,451 l/h). Temperature was controlled by an aquarium heater (300 W, 20–35°C) and a refrigerator cooler (connected to the pump). A plastic sheet was used to cover the tank to avoid evaporation. After one day of acclimation at 25°C (arrow in Fig. 1), the temperature was elevated by 2°C per day. Upon reaching the desired temperature (i.e., 31°C), corals were cultured under 400 µmole m^{-2} s^{-1} artificial light (12/12 h, L/D cycle) for 5 days. Light was provided at a 4-cm distance from the seawater surface, the light itself being held in a plastic holder (made from a water pipe). The
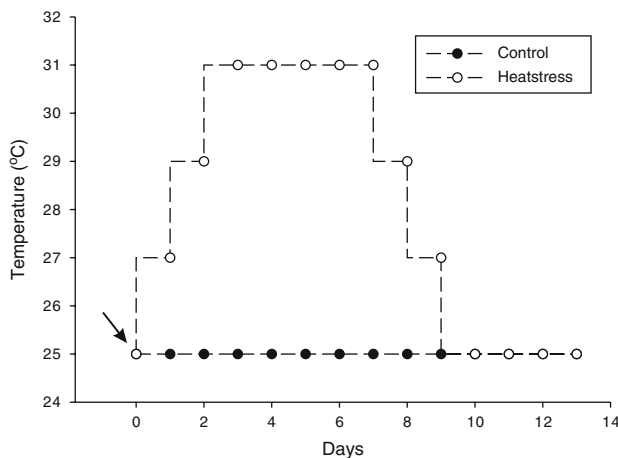
Fig. 1 Temperature design for heat stress-induced coral bleaching. Colonies of *E. glabrescens* were first cultured in seawater at 25°C for 24 h for acclimation (see arrow), and the water temperature was then elevated at a rate of 2°C/day to 31°C (open circles). Colonies were treated for 5 days at 31°C, followed by a gradual temperature decrease (−2°C/day) to 25°C; they were then cultured at 25°C with fresh filtered seawater for another 4 days before the experiment at day 13. The control experiment was performed similarly but without the temperature increase (filled circles). The degree of bleaching was determined by chlorophyll *a* content measurement as described in the "Materials and methods" section

light intensity at the seawater surface was measured using a light meter (TES-1339, TES Electrical Electronic Corp., Taiwan). Afterward, the temperature was reduced to 25°C stepwise (−2°C per day) for recovery. Surviving colonies were bleached by day 13 and were then used for experiments. Based on chlorophyll measurements, bleached corals with average chlorophyll *a* concentrations of ~ 10–$50\ \mu g\ mg^{-1}$ protein and $\leq 10\ \mu g\ mg^{-1}$ protein were classified as "partially bleached" and "severely bleached," respectively. The healthy colonies used as controls were treated similarly but without the temperature increase, and contained chlorophyll *a* at ~ 70–$100\ \mu g\ mg^{-1}$ protein.

Preparation of isolated symbiotic gastroderm cells (SGCs)

Isolated symbiotic gastrodermal cells were obtained from amputated tentacles turned inside-out according to the published procedure (Chen et al. 2005). Cells were then suspended in filtered seawater (FSW) with final cell concentration ~ 1–$2 \times 10^6\ ml^{-1}$. The intactness of their plasma membranes was then examined (Chen et al. 2005).

Fluorescence microscopy and dual-emission ratiometric imaging of lipid dynamics in LBs

Stock Nile red (9-diethylamino-5H-benzo[α]phenoxazine-5-one, from Sigma–Aldrich, St. Louis, MO, USA) was

prepared at $0.5\ mg\ ml^{-1}$ in acetone and stored at 4°C for use. Amputated tentacles were incubated in ASW containing 2.5–$5\ \mu g\ ml^{-1}$ of Nile red (final acetone concentration <1%) at room temperature for 30 min. Extracellular Nile red was then removed by washing with FSW. Taking advantage of the elastic properties of the epidermis, pure gastrodermis was then obtained by gently pressing the amputated tentacles using straight and curved highly polished iris forceps under a stereomicroscope (Stemi 2000, Zeiss, Oberkochen, Germany). The isolated gastrodermis was then placed onto a concave slide and covered with a 22×22-mm coverslip for observation.

Dual-emission of Nile red ratiometric imaging was performed using an upright microscope (Axioskop 2 plus, Zeiss) equipped with a Plan-Neofluar 40x (NA 0.75) objective and epifluorescence optics. A CCD camera (CoolSNAP-Pro *cf* with a 700-nm cut-off, Photometrics, Tucson, AZ, USA) was connected to the microscope along with a $0.63\times$ video adaptor for obtaining images. To minimize photobleaching, samples were first focused under halogen light differential contrast microscopy (DIC). Nile red fluorescent images were then acquired using the appropriate filters ("Red" emission: 575–640 nm and "Green" emission: 515–565 nm), under attenuated blue light excitation (465–495 nm) (Table 1). Fifteen sets of fluorescence images (triplicates of 5 image sets per tentacle; each set contained DIC, "red," "green" and DAPI images) of Nile red-stained tissues were taken (~ 50 ms exposure) and digitized (12- to 8-bit, saved in TIFF format) using Image-Pro plus 6.0 (Media Cybernetics, Bethesda, MD, USA), which was configured to a gray scale 12-bit depth and 696×520 pixels of capture area. Exposure time of 50 ms for acquiring fluorescent image ensured fluorescent intensity per pixel in each image to be below the saturation level (data not shown).

For R/G ratio imaging analysis, all procedures were performed using Metamorph 6.3 software (Molecular Devices, Sunnyvale, CA, USA) according to a modified procedure from previous reports (Chen et al. 1997; Chen 2002). Threshold levels of fluorescent images and their masking were created such that specific lipid bodies of hosts (denoted as "host LBs") or symbionts (denoted as "sym LBs") were selected to calculate the ratio of "red" to "green" fluorescence (denoted as the "R/G ratio") in LB populations. Distributions of the R/G ratio in the LB

Table 1 Optical filter sets for Nile red ratiometric imaging

Channel	Zeiss filter set component		
	Excitation filter	Beam splitter	Emission filter
Green	BP 480 ± 15	FT 510	BP 515–565
Red	BP 480 ± 15	FT 560	BP 575–640

Unit for all filters is wavelength (nm); *BP*, Bandpass

population were then logged into to Excel (Microsoft) and plotted in a histogram using SigmaPlot 10 (Systat Software Inc., San Jose, CA, USA).

Measurement of size and number of LBs in hosts and symbionts by imaging analyses

In order to count the number of LBs and determine their size (i.e., diameter) from the acquired Nile red images, the ratio of actual size (length) to pixel was first determined by distance calibration using an image acquired from a micrometer slide (0.01-mm division) at $400\times$ magnification with the $0.63\times$ video adaptor. The ratio of length/pixel in images of a 696×520 resolution was 0.37 (i.e., one pixel $= 0.37$ μm). The size distribution of the LBs was then determined by measuring their mask area using the integrated morphometry measurement tool provided in Metamorph software. Due to the distinct fluorescence of symbionts under the DAPI filter set, the numbers of symbionts in the acquired images were measured by counting the integrated pixels of objects selected by the symbionts mask using the DAPI filter.

Liposome assay

Liposomes containing polar and neutral lipids in various molar ratios were prepared by a modified ethanol injection procedure (Kremer et al. 1977) as follows. A polar lipid mixture (cholesterol:phosphatidyl ethanolamine: lecithin:lysolecithin, 1:1:1:1 by weight, stock 0.25 mg ml^{-1} in ethanol; Matreya, Pleasant Gap, PA, USA) and a neutral lipid mixture (cholesteryl palmitate:tripalmitin:palmitic acid:cholesterol, 1:1:1:1 by weight, stock 0.25 mg ml^{-1}) were mixed in various molar ratios based on their cholesterol moles (polar:neutral $= 1:0$, 4:1, 1:4, and 0:1) and dissolved in 100 μl ethanol or acetone/ethanol. This ethanol or acetone/ethanol solution was then injected into 1 ml of solution containing 10 mM PBS and 3.14 μM Nile red while vortex mixing. The emission spectra of these liposome–Nile red solutions were then examined by spectrofluorometer (F-2500, Hitachi, Tokyo, Japan) under 488 nm excitation.

LB purification and lipid analysis

In order to avoid nematocyst discharge, which interferes with the LB purification procedure, the white tip of amputated tentacles, which contains the most nematocysts, was first removed. After rinsing in FSW, ~ 30–50 *E. glabrescens* tentacles were homogenized using a plastic grinder on ice in 2–3 ml isotonic ASW containing protease inhibitors (Complete, protease inhibitor cocktail tablets; Roche Applied Science, Indianapolis, IN, USA) and 250 mM sucrose. The homogenate was centrifuged ($500\times g$ for 10 min) to pellet the symbionts. The supernatant

fraction containing host LBs was then transferred to a 1.5 ml eppendorf tube and overlayed with PBS solution. Here, the volume of this supernatant was normalized by its protein content using BCA protein assay (Pierce, Rockford, IL, USA). This solution was then centrifuged at $10,000\times g$ for 30 min to isolate the host lipid bodies. For symbiont lipid bodies (i.e., sym LBs) isolation, pelleted symbionts were first washed with ASW to eliminate host contamination. Symbionts were then suspended in PBS containing 250 mM sucrose and homogenized by a mini-BeadBeater (Biospec, India) for 5 min using glass beads (acid-washed 425–600 μm; Sigma). Afterward, sym LBs were isolated as per the method used for host LBs isolation.

Both host and sym LBs were extracted by a modified Bligh and Dyer (1959) method using 0.9% NaCl and 10 mM HCl in the aqueous phase (Dubinsky and Aaronson 1978). The extracted lipids of LBs from corals with different endosymbiotic status were standardized per gram tissue protein, and were analyzed by high performance thin-layer chromatography (HPTLC). The lipid standards listed as follows were used as markers: polar lipid mix (cholesterol, phosphatidyl ethanolamine, lecithin, lysolecithin; 1:1:1:1 by weight, 0.25 mg ml^{-1}; Matreya); neutral lipid mixture (cholesteryl palmitate, tripalmitin, palmitic acid, cholesterol; 1:1:1:1 by weight, 0.25 mg ml^{-1}); triglyceride mixture (tricaprin, tricaprylin, trilaurin, trimyristin, tripalmitin; 1:1:1:1:1 by weight, 0.2 mg ml^{-1}; Supelco, St. Louis, MO, USA); cholesterol (0.16 mg ml^{-1}; Matreya). After development in chromatographic solvent system (hexane/chloroform/acetic acid 80/20/1 v/v/v), the separated lipids on HPTLC plates were stained by Coomassie blue (Nakamura and Handa 1984), quantified using a scanner (Epson Perfection 1270; Epson America, Inc., Long Beach, CA, USA), and analyzed using Metamorph software. The absolute amounts of lipid species in the lipid bodies were determined by reference to known amounts of lipid standards chromatographed and analyzed on the same plate.

Miscellaneous procedures

The chlorophyll *a* concentration of samples (mg l^{-1}) was measured according to reported procedure (Jeffrey and Humphrey 1975). To simultaneously stain both the LBs and the nucleus, amputated tentacles were incubated with FSW containing Nile red (15.7 μM) and Hoechst 33342 (16 μM) at room temperature for 10 min. Isolated gastrodermis was then examined under Cy3 and DAPI filters.

Statistics

All statistical analyses were performed using SigmaStat 3.5 software (Systat software). Student's *t*-test was used to compare the statistical significance between two groups, and

one-way analysis of variance (ANOVA) was used to compare the statistical significance among groups that only contained one independent variable. The post hoc Tukey's test was employed for multiple comparisons among means from significant ANOVA tests (Day and Quinn, 1989). Linear regression was used when the compared groups had a continuous dependent variable. A P value of less than 0.05 or 0.1 ($P < 0.05$ or $P < 0.1$) was considered to indicate significance. The results were expressed as means ± SEM (the standard error of the mean).

Results

Lipid bodies in the gastrodermis and symbiotic gastrodermal cells

Nile red, a fluorescent lipophilic probe, was used to identify the distribution of LBs in algal and host cells. It has been used to detect lipids both in vitro and in vivo as it exhibits high affinity, specificity, and sensitivity to the degree of hydrophobicity of lipids (Greenspan and Fowler 1985; Greenspan et al. 1985; Kwok and Wong 2005; Diaz et al. 2008). The large tentacles of the hermatypic coral *E. glabrescens* were used for investigating the role of LBs in the present study due to the ease of separating its tissue layers (Peng et al. 2008), which allowed the tissue distribution of LBs to be clearly demonstrated. First, discernible LBs identified by the Nile red staining were found to exist only in the gastrodermis (panels a–a′), and not in the epidermis (panels b–b′) (Fig. 2). In the gastrodermis, in addition to various cells types including the symbiotic gastrodermal cells (SGCs, i.e., gastrodermal cells that contain the *Symbiodinium*, sym) and a particular type of nematocyte (nc), numerous phase-contrast vacuoles distributed near the symbiont were observed (open arrows, Fig. 2a). These vacuoles were labeled by Nile red and are thus identified as "host LBs" (open arrows, Fig. 2a′).

Fig. 2 Distribution of lipid bodies (LBs) in tissues and cells. The gastrodermis (panels a–a′), epidermis (panels b–b′), and isolated symbiotic gastrodermal cells (panels c–c′) were prepared and stained with Nile red and Hoechst 33342 as described in the "Materials and methods" section. The distributions of LBs were then examined by DIC (panels a, b, and c) and fluorescence (panels a′, b′, and c′) microscopy. Co-localization of Nile red staining in host LBs is indicated by open arrows (panels a–a′ and c–c′). Symbiont LBs stained by Nile red are indicated by filled arrows (panels a′ and c′). Arrowheads in panels a–a′ indicate the location of nuclei as stained by Hoechst 33342. Abbreviations: *sym*, Symbiont; *nc*, Nematocyte; *n*, Nucleus of symbiotic gastrodermal cell
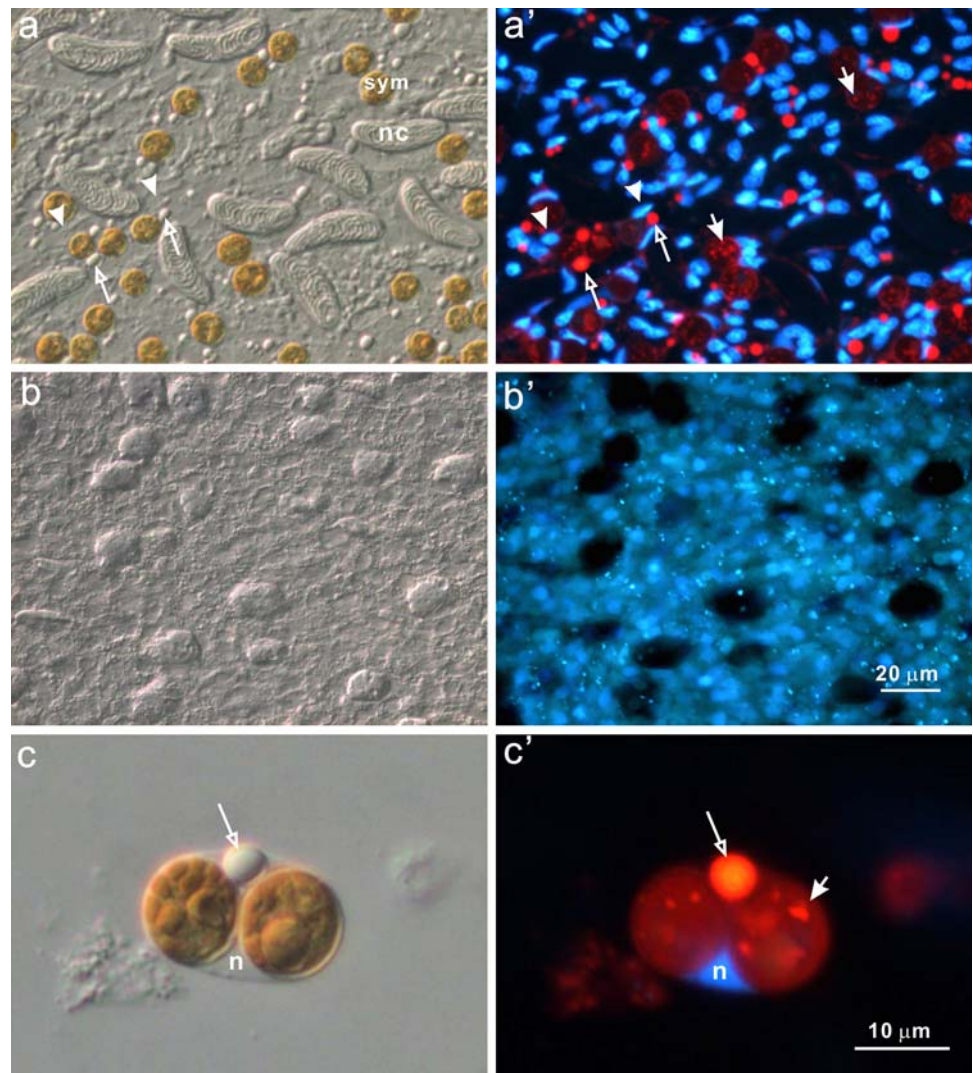
Besides the larger host LBs (~3.5 μm in diameter), smaller LBs (i.e., "sym LBs") were also observed inside the symbionts (filled arrows in Fig. 2a'; ~1.2 μm in diameter). In tissues doubly stained with both Nile red and Hoechst 33342, the LBs were clearly distinguishable from the host cell nucleus (blue fluorescence as indicated by arrowheads in Fig. 2a'). The exact distribution of host LBs in the gastrodermis was further examined on isolated symbiotic gastrodermal cells (SGCs), as shown in Fig. 2c–c'. In most isolated SGCs containing single or multiple numbers of symbionts, one to two host LBs could be observed by both DIC and Nile red staining (open arrows, Fig. 2c–c'). The smaller "sym LBs" inside the symbiont could also be observed (filled arrow, Fig. 2c').

The dynamics of lipid body formation was explored in healthy corals and bleached corals in which bleaching was artificially induced by heat stress, as described in the "Materials and methods" section. Based on the chlorophyll a content (μg per mg protein), corals of differing endosymbiotic status were classified as "healthy" (82.17 ± 10.78 μg mg^{-1} protein), "partially bleached" (15.51 ± 3.49 μg mg^{-1} protein) and "severely bleached" (2.45 ± 1.52 μg mg^{-1} protein) (Table 2). As shown in Fig. 3, the densities of both the symbiont population and host LBs were highly positively correlated with endosymbiotic status ($R = 0.858$). Namely, the poorer the symbiotic status (i.e., bleaching), the lower the symbiont population and the fewer the host LBs. Compared with control healthy corals, there was an average reduction of 66.99 and 92.34% in symbiont population, and 32.43 and 84.46% in host LBs density, in partially bleached and severely bleached corals, respectively. This observation provides direct evidence that the formation of host LBs is closely related to the endosymbiotic status of corals.

Quantitative dual-emission ratiometric imaging of LB lipid composition in live gastrodermis of differing endosymbiotic status

Nile red has long been considered an important solvatochromic dye for studying the dynamic change of polar and neutral lipids by flow cytometry (Greenspan et al. 1985; Kwok and Wong 2005). Due to its emission and absorption changes in different environments, the fluorescence shifts
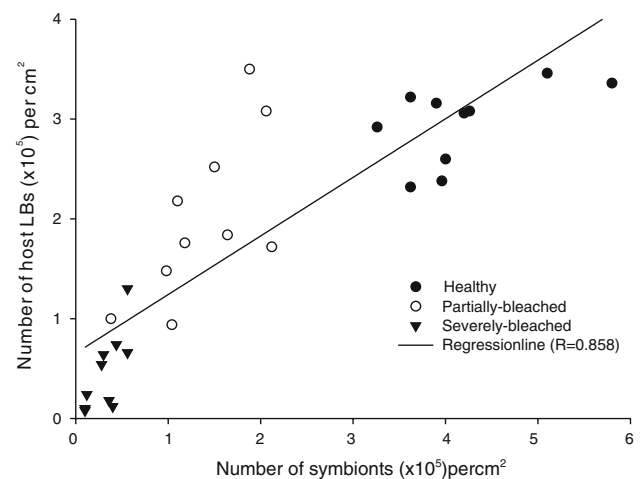

Fig. 3 Correlation between densities of host LBs and symbionts in corals of differing symbiotic status. Data were collected by examining ten ($N = 10$) micrographs acquired by imaging of isolated gastrodermis from corals in a healthy (*filled circles*), partially bleached (*open circles*) or severely bleached (*filled triangles*) condition. Densities of the host LBs and symbionts were determined by analyzing their numbers per cm^2 tissue area

can be used to quantify the surrounding lipid composition (Greenspan and Fowler 1985). As a consequence, Nile red was used in the present study to develop live cell imaging, not only to investigate the in situ LB distribution, but also to quantify the lipid compositional changes inside LBs.

To verify the feasibility of dual-emission ratiometric measurement, the spectral shift of Nile red fluorescence in liposomes of lipids with different polarities was first examined by spectrofluorometric analysis, as shown in Fig. 4. In the absence of liposomes (i.e., in phosphate-buffered saline only), Nile red was basically non-fluorescent under 488 nm excitation. Nile red fluorescence significantly increased upon the addition of liposomes; furthermore, there was an emission spectral shift from the green region (515–565 nm) to the red region (575–640 nm) of wavelength in liposomes containing increasing molar ratios of polar lipid:neutral lipid mixtures (i.e., from 0%, 1:4 (20%), 4:1 (80%) to 100%). Namely, there was an emission spectral change, with the main peak in the red region shifting from 575 nm to 595 nm (see the open arrow), accompanied by a decrease in fluorescence

Table 2 Degree of bleaching versus chlorophyll a concentration

	Healthy	Partially bleached	Severely bleached
chl a/protein (μg mg^{-1})	82.17 ± 10.78	15.51 ± 3.49	2.45 ± 1.52
Reduction of chl a (%)	0%	81.12%	97.02%

The degree of symbiont loss after bleaching was monitored by calculating the chlorophyll a content of the total proteins of the amputated tentacles (chl a/protein, μg mg^{-1}). Data are presented as mean $\pm$ SEM averaged from six ($N = 6$) repetitions. Reduction of chl a (%) is the average chl a reduction as compared with that of the healthy control corals
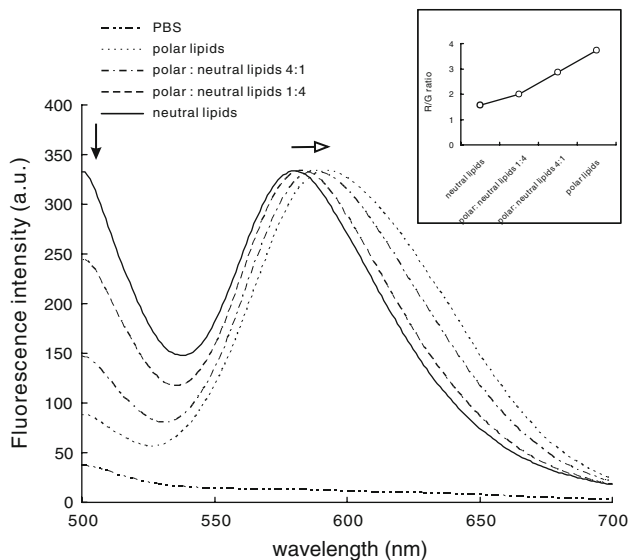
Fig. 4 Spectrofluorometric analysis of Nile red fluorescence in liposomes containing varying amounts of polar versus neutral lipid mixtures. Under blue light excitation (488 nm), the spectrum of Nile red fluorescence shifted from the green (G, 515–565 nm) to the red (R, 575–640 nm) region of wavelength when the molar percentage of polar lipids increased in the liposomes (see open arrow). Note that in the green region, the fluorescence decreased when the percentage of polar lipids increased (see arrow). The inset shows the effect of polar versus neutral lipids molar percentage on the ratio of integrated red (R, 575–640 nm) over green (G, 515–565 nm) fluorescence. (a.u., arbitrary fluorescence unit)

intensity in the green region of wavelength (515–565 nm, see the filled arrow). This spectral shift of Nile red in liposomes containing different lipids versus lipid molar ratio was then quantified by measuring the ratio of integrated fluorescence intensity of the red (i.e., 575–640 nm) over the green (515–565 nm) region of wavelength, or the "R/G ratio" (inset, Fig. 4). The higher the polar lipid concentration, the larger the R/G ratio. This in vitro assay demonstrated the usefulness of in situ ratiometric imaging of LBs using Nile red.

The R/G ratios of Nile red fluorescence in the LB population of live gastrodermis from corals with different symbiotic status (i.e., "healthy", "partially bleached" or "severely bleached") were then measured by quantitative ratiometric microscopy, where "host LBs" are separated from "sym LBs" by imaging analysis (see "Materials and methods" section). The concentration of acetone in the diluted Nile red stock solution was less than 1% (see the "Materials and methods" section), and showed no effect on the R/G ratio measurement (data not shown). As shown in Fig. 5, there were dynamic changes in the R/G ratio of LB populations depending on the symbiotic status. First, the R/G ratio of the host LB population increased upon bleaching, as shown by the right-shift of the R/G distribution

(open arrows, Fig. 5b–c) and the increase in the peak value (filled arrows) from 1.07 (healthy, Fig. 5a) to 1.27 (partially and severely bleached, Fig. 5b–c). However, in the symbiont, the R/G ratio of the LB population left-shifted toward lower values (open arrows, Fig. 5b'–c') after bleaching, with the peak value decreasing from 1.37 (healthy, Fig. 5a') to 1.27 (partially and severely bleached, Fig. 5b'–c'). These results indicated that changes in symbiotic status reflected upon the lipid compositional changes in LBs of both host cells and their symbiont *Symbiodinium*. The R/G ratio in host LBs increased as a result of bleaching, indicating a relative decrease in neutral lipids accumulation within. On the other hand, relative increase in neutral lipids accumulation in symbionts LBs resulted in gradual decrease of R/G ratio. The relative lipid compositional changes in LBs as shown by the changes in the Nile red R/G ratio were confirmed by comparative lipid analysis using cellular phospholipids (PLs) and triacylglycerols (TAGs) as markers for the polar and neutral lipids, respectively (Table 3). In host LBs, the concentrations of both PLs and TAGs decreased from 24.77 ± 0.82 to 21.56 ± 1.97 (ng μg^{-1} proteins) and 20.17 ± 0.17 to 16.05 ± 0.52 (ng μg^{-1} proteins), respectively, after bleaching, resulting in an significant increase in the PLs:TAGs ratio (i.e., polar:neutral) from ~ 1.23 to ~ 1.35 ($P < 0.1$). Here, TAGs content in host LBs of partially bleached corals was significantly lower than that in healthy control ($P < 0.05$). On the other hand, there are increases rather than decreases of both PLs and TAGs in sym LBs upon bleaching. The lipid composition change results in a decrease in the polar:neutral lipids ratio from ~ 1.57 to ~ 1.46. Here, TAGs content in symbiont LBs of partially bleached corals was significantly higher than that in healthy control ($P < 0.1$). The lipid content of LBs in severely bleached corals was not analyzed due to the low amount of available LBs (data not shown).

However, the patterns of R/G ratio shift differed in corals under continual (i.e., 22 h) light or dark treatment from those undergoing the bleaching, as shown in Fig. 5d–d' (light-treated) and Fig. 5e–e' (dark-treated). In both light- and dark-treated corals, there was no significant spectral shift in the R/G ratio of the host LB population, and the peak values of the R/G ratio remain at 1.07, as for the healthy corals (see filled arrows in Fig. 5a, d, e). On the other hand, the R/G ratios of the symbiont LB populations shifted toward higher values (i.e., right-shifted, see open arrows in Fig. 5d', e') although not significantly, with the peak values increasing to 1.56. These observations of the dynamic R/G ratio distribution in both host and sym LBs, as shown in Fig. 5 indicated that the lipid compositional changes in LBs as a result of bleaching and continual light/dark treatment were different in mechanism.

Fig. 5 Dynamic change in the R/G ratio of LBs with differing symbiotic status. Gastrodermis isolated from corals of differing status (healthy, a–a'; partially bleached, b–b'; severely bleached, c–c'; light-treated, d–d'; dark-treated, e–e') were incubated in Nile red to stain the LBs (see "Materials and methods"). The R/G ratios of Nile red fluorescence were then determined for both host LBs (panels a–e) and symbiont LBs (panels a'–e') separately. The numbers of host and sym LBs determined are shown in Table 4 (see "*n*" value). The R/G values were then plotted as a function of the percentage of LB area. The filled arrows in each panel indicate the peak value of R/G in the total population, while the open arrows indicate the direction of the population shift in comparison with the control healthy corals (panels a–a')
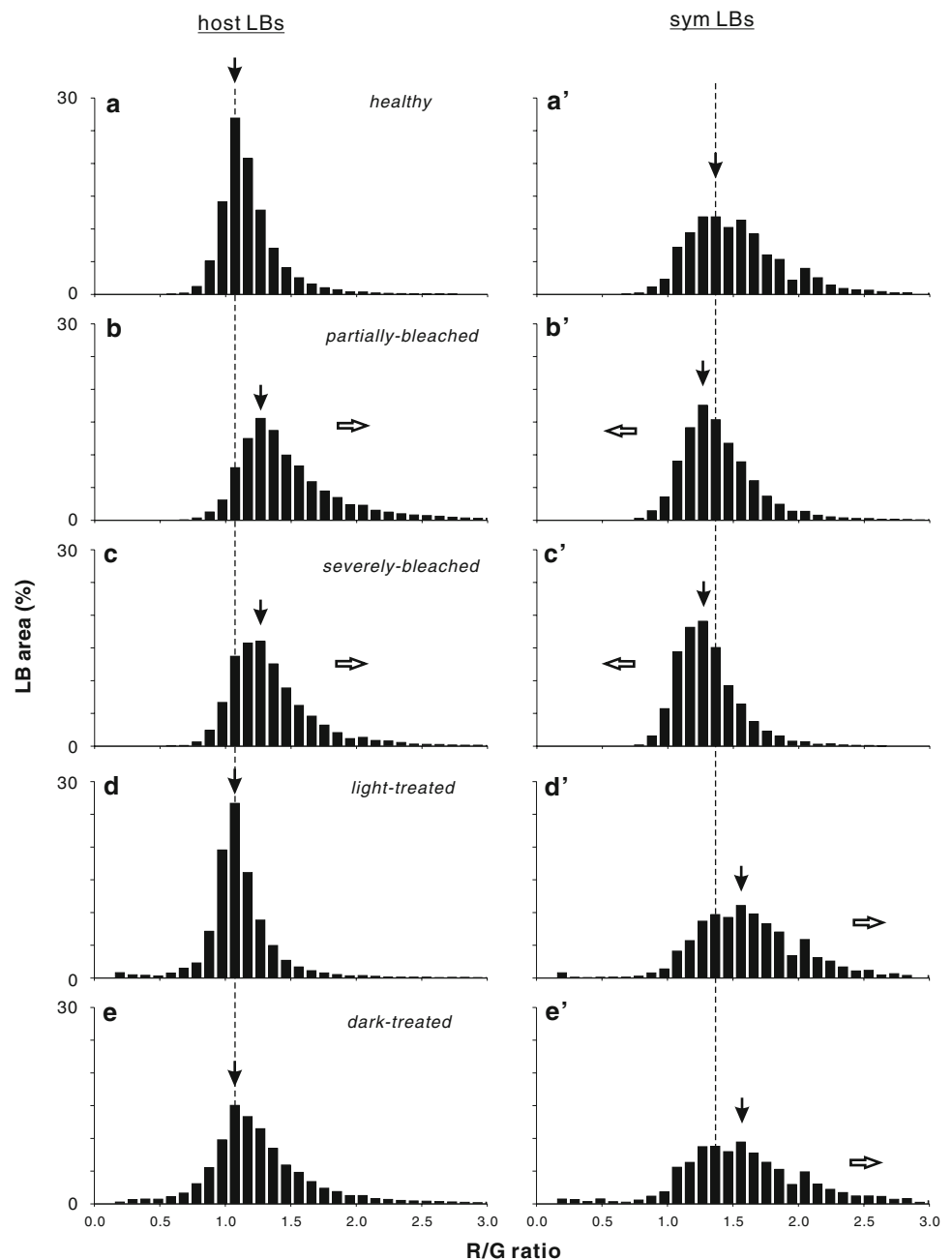
Analyses of LBs distribution, size and R/G ratio images with differing endosymbiotic status

The spatial distributions and sizes of LBs in the gastrodermis with differing endosymbiotic status were further examined using imaging analysis after Nile red staining (Table 4 and Fig. 6). In the healthy coral, host LBs were prominent and measured 3.47 ± 0.04 μm in diameter, as shown by Nile red staining (Fig. 6a, open arrows; Table 4). Symbiont LBs were found to be smaller in size (1.26 ± 0.01 μm, Table 4; filled arrows in Fig. 6a). Ratiometric images of the R/G ratio indicated that symbiont

LBs exhibited a larger R/G ratio than those of host LBs (see the selected inset and its ratiometric image). However, bleaching (see Fig. 6b for severely bleached corals) resulted in significant changes in the LBs of the host and symbionts. First, not only did the number of host LBs decrease (see Fig. 3), but their sizes also significantly decreased (Table 4; 2.25 ± 0.08 μm in diameter) in comparison with those in healthy control (3.47 ± 0.04 μm) ($P < 0.001$). Second, the size of the sym LBs significantly increased from 1.26 ± 0.01 μm to 2.44 ± 0.06 μm in diameter (also see Table 4), resulting in a redistribution of Nile red staining from the host to the symbiont (filled

Table 3 Lipid contents of the host and symbiont LBs during bleaching

Lipid species	Host LBs		Sym LBs	
	Healthy (Control)	Partially bleached	Healthy (Control)	Partially bleached
PLs	24.77 ± 0.82	21.56 ± 1.97	190.08 ± 39.79	254.62 ± 45.40
TAGs	20.17 ± 0.17	16.05 ± 0.52[a]	121.59 ± 3.46	172.12 ± 22.00[b]
PLs/TAGs ratio	1.23 ± 0.05	1.35 ± 0.17*	1.57 ± 0.33	1.46 ± 0.10

Host and sym LBs were isolated from host tissues and symbionts, and their lipids were analyzed by HPTLC (see "Materials and methods" section). Lipid contents are expressed as lipid/protein (ng μg^{-1}). PLs, phospholipids; TAGs, triacylglycerols; Data are presented as mean±SEM (N=3)

* Statistically significant ($P < 0.1$) of PLs/TAGs ratio in Host LBs between Healthy and Partially bleached corals

[a] Statistically significant ($P < 0.05$) of TAGs in Host LBs between Healthy and Partially bleached corals

[b] Statistically significant ($P < 0.1$) of TAGs in Sym LBs between Healthy and Partially bleached corals

Table 4 Changes in LB size of host and symbionts with differing symbiotic status

		Healthy	Bleaching		Continual light/dark (22 hrs)	
			Partial	Severe	Dark	Light
Host LBs	Size	3.47 ± 0.04[a] (n = 1,385)	2.36 ± 0.04[b] (n = 989)	2.25 ± 0.08[b] (n = 219)	3.28 ± 0.06[c] (n = 863)	3.09 ± 0.04[c] (n = 938)
Sym LBs	Size	1.26 ± 0.01[a'] (n = 4,913)	1.94 ± 0.03[b'] (n = 2,357)	2.44 ± 0.06[c'] (n = 642)	1.12 ± 0.01[d'] (n = 2,417)	1.17 ± 0.01[d'] (n = 4,015)

The total numbers (n) of host or symbiont LBs were measured and data are presented as mean ± SEM. Superscript a–c and a'–d' denote statistical significance between different symbiotic statuses for "Host LBs" and "Sym LBs," respectively ($P < 0.001$). Size (diameter, μm); LB, lipid body

arrows, Fig. 6b). Third, ratio imaging indicated that there was a drastic increase in the R/G ratio of host LBs (see open arrows in the selected inset, Fig. 6b), which was consistent with the R/G ratio increase in the total host LB population, as shown in Fig. 5. The dynamic changes in the distribution, size and R/G ratio of LBs of the bleached corals were totally different from those of continual light- and dark-treated corals (Fig. 6c, d; Table 4). In both light- and dark-treated corals, the size of host LBs decreased from 3.47 ± 0.04 (Healthy control) to 3.09 ± 0.04 (Light treatment) and 3.280.06 μm (Dark treatment), although not as significant as changes in bleached corals (Table 4). Meanwhile, the size of sym LBs further decreased, rather than increased as those in bleached corals, from 1.26 ± 0.01 (Healthy control) to 1.17 ± 0.01 (Light treatment) and 1.12 ± 0.01 μm (Dark treatment). This resulted in no Nile red staining redistribution in either the light- or dark-treated corals (Fig. 6c, d) in comparison with that in healthy control (Fig. 6a). In both cases, the R/G ratio of the host LBs remained similar to those of the control (see the selected insets in Fig. 6c, d).

Discussion

The molecular mechanism responsible for endosymbiosis regulation during cnidaria–dinoflagellate association is still unclear after five decades of investigation. Endosymbiosis had been shown to be initiated by the phagocytosis of *Symbiodinium* into gastrodermal cells of host animals (Hohman et al. 1982). Both membrane and lipid trafficking should play critical roles in initiating and maintaining the mutualistic interaction between the host cells and their intracellular symbionts. However, few experimental data are currently available to provide exclusive insights. This is basically due to several experimental bottlenecks that are difficult to resolve at the moment, including (i) the complexity of the cell types and a lack of in vitro cell cultures, and (ii) the absence of a membrane purification strategy that allows the separation of host and symbiont membrane fractions. With the former, cellular and molecular events of membrane systems in gastrodermal cells cannot be specified for examination due to interferences from other cell types in animal tissues. With the latter, membrane inter-actions and lipid transportation between host gastrodermal cells and their intracellular symbionts cannot be analyzed. To circumvent these technical problems, we identify host LBs as one of the organelles correlated with symbiotic status by a novel ratiometric imaging method, and provide future research rationale that lipid trafficking between LBs of the host and symbiont can be examined in both live tissues and isolated gastrodermal cells. It is known that the symbionts, *Symbiodinium*, provide the host cells with photosynthetic products, or photosynthates; however, the

Fig. 6 Dynamic changes in size and number of host and symbiont LBs with differing symbiotic status. Panels a, b, c, and d are overlaid images of DIC and Nile red fluorescence (red) microscopies for healthy, partially bleached, light-treated, and dark-treated corals, respectively. Pseudo-color ratio images of the R/G ratio from selected regions (dash-line square) are shown in the right corner of each panel (bar in inset of panel d, 3 μm). The locations of host and symbiont LBs are indicated by open and filled arrows, respectively
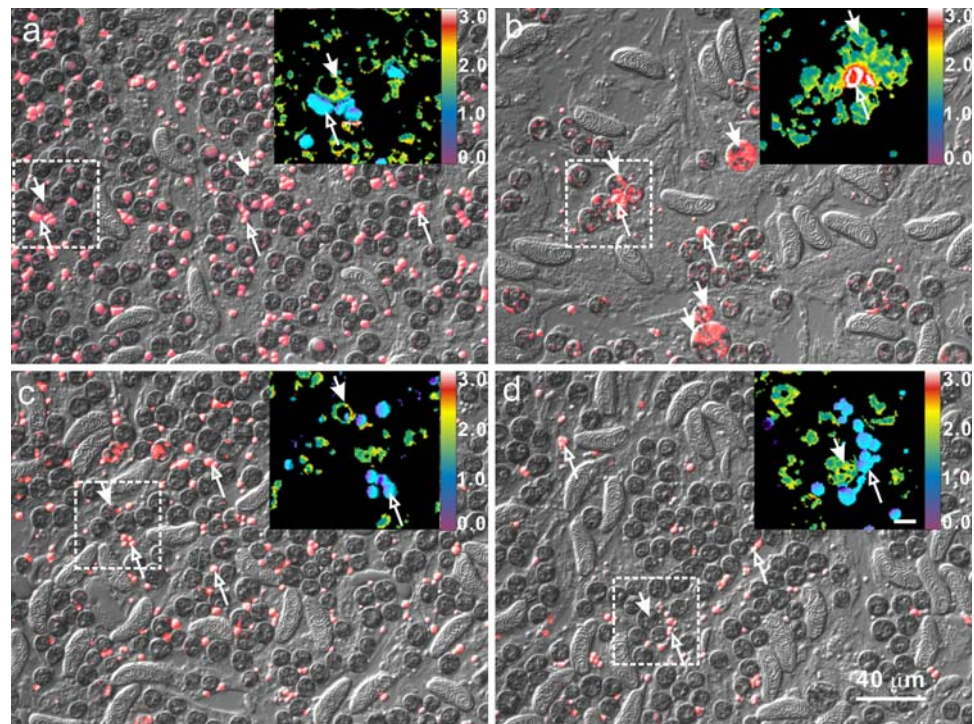
mechanism for the translocation of these photosynthates from the symbiont to the host remains unclear (Venn et al. 2008 for review). The idea that photosynthates such as lipids are exported to the host directly from the symbionts was initially based on the interpretation of an observation that certain "lipid droplets" are attached to the symbionts (Kellogg and Patton 1983; Patton and Burris 1983). However, these lipid droplets have since been identified as host cell nuclei due to their distribution being adjacent to the host cell nucleus (Gates and Muscatine 1992). In this study, we first identified and characterized host LBs in live tissues and cells, and provided evidence of the correlation of their lipid changes with differing symbiotic status.

Nile red (also know as Nile blue oxazone) has been used to investigate lipid dynamics in various mammalian and plant cells (Greenspan et al. 1985; Priscu et al. 1990; Elsey et al. 2007). It is a lipophilic and solvatochromistic lipid indicator that exhibits shifts of fluorescent emission from red (excitation/emission: 540 nm/590 nm) to yellow (excitation/emission: 460 nm/535 nm) depending on the increasing hydrophobicity of lipids (Greenspan and Fowler 1985). Polar lipids (e.g., phospholipids) are stained in red upon 540 nm excitation, whereas neutral lipids (e.g., esterified cholesterol and triglycerides) are stained in yellow upon 460 nm excitation. This property allows its wide application in monitoring lipid changes in live cells and tissues (Fowler and Greenspan 1985; Klinkner et al. 1997). It has been extensively used in quantifying lipid contents by flow cytometry in mammalian cells (Greenspan et al. 1985) and dinoflagellates (Kwok and Wong 2005). Ratio

imaging using fluorescent indicators has been widely applied in studies of various molecular changes in living cells (Arndt-Jovin et al. 1985 for review), such as cytoplasmic pH (Bright et al. 1987), calcium (Knot et al. 2005), and lipids (Chen et al. 1997). It has many advantages over intensity-base imaging. For example, errors in fluorescence measurements resulting from leakage, photobleaching, cell thickness, and nonuniform indicator distributions can be corrected using excitation or emission ratio (Bright et al. 1987). Ratiometric imaging using Nile red for intracellular lipids has been recently explored based on red (excitation/emission: 540 nm/590 nm) versus yellow (excitation/emission: 460 nm/535 nm) fluorescence for polar versus neutral lipids, respectively (Diaz et al. 2008). However, spectrofluorometric quantification had shown that the above-mentioned excitation/emission wavelengths of Nile red were not specific enough for polar and neutral lipids (Alonzo and Mayzand 1999). Namely, there is spectral overlap where Nile red fluorescence of polar lipids could be detected under neutral lipid conditions (i.e., excitation at 460 nm) and similarly, neutral lipid Nile red fluorescence could be recorded under polar lipids conditions (i.e., excitation at 540 nm). This spectral overlap would definitely add complications to estimate relative polar versus neutral lipids ratio during the ratiometric measurement. As a consequence, in the present study, a dual-emission ratiometric imaging under a single excitation was developed to diminish this overlap. Here, under the blue excitation at 480 ± 15 nm, the polar lipids were identified by Nile red fluorescence at 575–640 nm (i.e., the "red" image, "R")

while neutral lipids were identified at 515–565 nm (i.e., the "green" image, "G"; see also Table 1). The feasibility of this dual-emission ratiometric measurement on Nile red fluorescence was then directly verified using a liposome assay (Fig. 4), demonstrating its ability to specifically monitor relative lipid compositional changes in host and symbiont LBs in live coral tissues during endosymbiosis.

In summary, the results showed that both morphological and compositional changes of LBs were regulated according to symbiotic status during the coral–dinoflagellate association (Fig. 7). First, host LBs are characteristic organelles in the symbiotic but not aposymbiotic gastrodermal cells, whose number (see Fig. 3) and size (see Table 4) significantly decrease as a result of bleaching and continual light and dark treatments. On the other hand, the size of symbiont LBs significantly increased as a result of bleaching but not continual light and dark treatments (Table 4). Secondly, changes in the R/G ratio of Nile red fluorescence indicated that, as a result of bleaching, there was an increase in the relative ratio of polar versus neutral lipids (P/NP) in host LBs, while there was a decrease in the relative P/NP ratio in symbiont LBs. Comparative biochemical analysis using standard phospholipids and triacylglycerols confirmed the change of relative P/NP in both host and symbiont LBs (Table 3), although the exact concentration changes of different lipid species in these LBs as a result of bleaching remain to be elucidated. The opposite R/G ratio and relative P/NP ratio changes between host and symbiont LBs after bleaching indicates that there is a directional lipid trafficking from the symbiont LBs to the host LBs (i.e., from pathway A to B in Fig. 7) during endosymbiosis. During the

stable endosymbiosis, the metabolites are mainly translocated to the host, and few lipids accumulate in the symbionts according to the present and previous studies (Trench 1971; Wang and Douglas 1997; Biel et al. 2007). This led to a smaller R/G ratio (i.e., relative smaller P/NP) in host LBs, indicating comparatively higher neutral lipids contents in host LBs, whereas bleaching (pathway C in Fig. 7) blocks the trafficking pathway B, resulting in increases in size of the symbiont LBs and relative higher neutral lipid accumulation (i.e., smaller R/G ratio or relative P/NP ratio) within (see also Fig. 6b, Tables 3 and 4). Thirdly, continual dark or light treatments did not alter the relative lipid distribution and R/G ratio of the lipid body staining in both host and symbiont LBs, strongly indicating that lipid metabolisms (or catabolism) in both host and symbiont LBs (see filled and open arrows around host and sym LB, respectively, in Fig. 7) are distinct pathways from lipid trafficking between symbiont LBs and the host LBs (i.e., pathways A to B in Fig. 7). The conclusion from these findings is that the endosymbiosis is regulated both by lipid trafficking between host and symbiont LBs and by lipid metabolisms inside the individual host and symbiont LBs.

Inside coral symbionts *Symbiodinium* sp. and mammalian cells, lipid accumulation that led to the formation of large amounts of lipid droplets was considered to be pathological (Franklin et al. 2004; Turró et al. 2006). Based on the present R/G ratiometric analysis and comparative lipid analysis (Fig. 5 and Table 3), in bleached corals, neutral lipids especially TAGs in host LBs significantly decreased, while those in symbiont LB increased. Although there was a similar trend in the change of phospholipids species (PLs) between host and symbiont LBs, it was not significant. These data indicate that TAGs were the major lipid species that showed significant redistribution between the host and symbiont LBs of different symbiosis status. It has been proposed that a stable symbiosis is maintained by sustained production of nutrients by the symbiont, which inactivates the host defense response; and the loss of nutrient production results in bleaching (Douglas 2003). It implicates that the TAGs trafficking between the symbiont and host LBs may be highly regulated for a stable endosymbiosis. Although the distribution of detailed lipid species in both host and symbiont LBs remains to be elucidated, the role of TAGs during the endosymbiosis may be more than just as energy resources or nutrients. TAG acts as a precursor of membrane lipid and can be used for conversion to PL in normal metabolism (Igal and Coleman 1996). The accumulation of TAG and cholesterol ester in the cells may activate apoptosis (Maxfield and Tabas 2005) and change the membrane integrity and photosynthetic activity in phytoplankton (Veldhuis et al. 2001).

Finally, the genesis of host LBs in the cytoplasm becomes another pivotal mechanism which requires
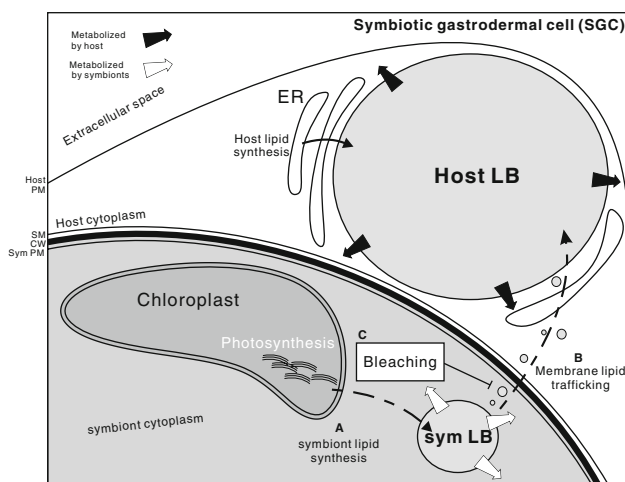

Fig. 7 A hypothetical model of lipid trafficking between host and symbiont LBs. Abbreviations: *ER*, Endoplasmic reticulum; *Host PM*, Host plasma membrane; *SM*, Symbiosome membrane; *CW*, Cell wall; *Sym PM*, Symbiont plasma membrane; *A*, Symbiont lipid synthesis pathway between the chloroplast and sym LBs; *B*, Membrane lipid trafficking pathway from the sym LB to the host LB; *C*, The bleaching process that blocks the pathway B

additional attention for future investigation. In mammalian cells, LBs have been shown to be assembled in the endoplasmic reticulum (Martin and Parton 2006). Nevertheless, the mechanism of host LBs assembly in cnidaria species remains completely unknown at the moment.

References

Alonzo F, Mayzand P (1999) Spectrofluorometric quantification of neutral and polar lipids in zooplankton using Nile red. Mar Chem 67:289–301

Arndt-Jovin DJ, Robert-Nicoud M, Kaufman SJ, Jovin TM (1985) Fluorescence digital imaging microscopy in cell biology. Science 230:247–256

Battey JF, Patton JS (1984) A reevaluation of the role of glycerol in carbon translocation in zooxanthellae-coelenterate symbiosis. Mar Biol 79:27–38

Biel KY, Gates RD, Muscatine L (2007) Effects of free amino acids on the photosynthetic carbon metabolism of symbiotic dinoflagellates. Russ J Plant Physiol 54:365–371

Bligh EG, Dyer WJ (1959) A rapid method for total lipid extraction and purification. Can J Biochem Physiol 37:911–917

Bright GR, Fisher GW, Rogowska J, Taylor DL (1987) Fluorescence ratio imaging microscopy: temporal and spatial measurements of cytoplasmic pH. J Cell Biol 104:1019–1033

Chen CS (2002) Phorbol ester induces elevated oxidative activity and alkalization in a subset of lysosomes. BMC Cell Biol 3:21–31

Chen CS, Martin OC, Pagano RE (1997) Changes in the spectral properties of a plasma membrane lipid analog during the first seconds of endocytosis in living cells. Biophy J 72:37–50

Chen CS, Yeh CC, Lin HP, Fang LS (2005) The use of a fluorescent membrane probe to identify zooxanthellae in hospite among dissociated endoderm cell culture from coral. Protoplasma 226:175–179

Coleman RA, Lee DP (2004) Enzymes of triacylglycerol synthesis and their regulation. Prog Lipid Res 43:134–176

Day RW, Quinn GP (1989) Comparisons of treatments after an analysis of variance in ecology. Ecol Monogr 59:433–463

D'Elia CF (1977) The uptake and release of dissolved phosphorus by reef corals. Limnol Oceanogr 22:301–315

D'Elia CF, Domotor SL, Webb KL (1983) Nutrient uptake kinetics of freshly isolated zooxanthellae. Mar Biol 75:157–167

Diaz G, Melis M, Batetta B, Angius F, Falchi AM (2008) Hydrophobic characterization of intracellular lipids in situ by Nile red red/yellow emission ratio. Micron 39:819–824

Douglas AE (2003) Coral bleaching-how and why. Mar Poll Bull 46:385–392

Dubinsky Z, Aaronson S (1978) Increase of lipid yields from some algae by acid extraction. Phytochemistry 18:51–52

Duncan RE, Ahmadian M, Jaworski K, Sarkadi-Nagy E, Sul HS (2007) Regulation of lipolysis in adipocytes. Annu Rev Nutr 27:79–101

Elsey D, Jameson D, Raleigh B, Cooney MJ (2007) Fluorescent measurement of microalgal neutral lipids. J Microbiol Methods 68:639–642

Fowler SD, Greenspan P (1985) Application of Nile red, a fluorescent hydrophobic probe, for the detection of neutral lipid deposits in tissue section: comparison with Oil red O. J Histochem Cytochem 33:833–836

Franklin DJ, Hoegh-Guldberg O, Jones RJ, Berges JA (2004) Cell death and degeneration in the symbiotic dinoflagellates of the coral *Stylophora pistillata* during bleaching. Mar Ecol Prog Ser 272:117–130

Gates RD, Muscatine L (1992) Three methods for isolating viable anthozoan endoderm cells with their intracellular symbiotic dinoflagellates. Coral Reefs 11:143–145

Greenspan P, Fowler SD (1985) Spectrofluorometric studies of the lipid probe, nile red. J Lipid Res 26:781–789

Greenspan P, Mayer EP, Fowler SD (1985) Nile red: a selective fluorescent stain for intracellular lipid droplets. J Cell Biol 100:965–973

Hohman TC, McNeil PL, Muscatine L (1982) Phagosome-lysosome fusion inhibited by algal symbionts of *Hydra viridis*. J Cell Biol 94:56–63

Igal RA, Coleman RA (1996) Acylglycerol recycling from triacylglycerol to phospholipid, not lipase activity, is defective in neutral lipid storage disease fibroblasts. J Biol Cell 271:16644–16651

Imanishi Y, Gerke V, Palcewski (2004) Retinosomes: new insights into intracellular managing of hydrophobic substances in lipid bodies. J Cell Biol 166:447–453

Jeffrey SW, Humphrey GF (1975) New spectrophotometric equations for determining chlorophylls a, b, c1 and c2 in higher plants, algae, and natural phytoplankton. Biochem Physiol Pflanz 167:191–194

Kellogg RB, Patton JS (1983) Lipid droplets, medium of energy exchange in the symbiotic anemone Condylactis gigantean: a model coral polyp. Mar Biol 75:137–149

Klinkner AM, Bugelski PJ, Waites CR, Louden C, Hart TK, Kerns WD (1997) A novel technique for mapping the lipid composition of atherosclerotic fatty streaks in en face fluorescence microscopy. J Histochem Cytochem 45:743–753

Knot HJ, Laher I, Sobie EA, Guatimosim S, Gomez-Viquez L, Hartmann H, Song LS, Lederer WJ, Graier WF, Malli R, Frieden M, Petersen OH (2005) Twenty years of calcium imaging: cell physiology to dye for. Mol Interventions 5:112–127

Kremer JMH, Esker MWJ, Pathmamanoharan C, Wiersema PH (1977) Vesicles of variable diameter prepared by a modified injection method. Biochemistry 16:3932–3935

Kwok ACM, Wong JTY (2005) Lipid biosynthesis and its coordination with cell cycle progression. Plant Cell Physiol 46:1973–1986

Liu P, Ying Y, Zhao Y, Mundy DI, Zhu M, Anderson RGW (2004) Chinese hamster ovary K2 cell lipid droplets appear to be metabolic organelles involved in membrane traffic. J Biol Chem 279:3787–3792

Martin S, Parton RG (2005) Caveolin, cholesterol, and lipid bodies. Semin Cell Dev Biol 16:163–174

Martin S, Parton RG (2006) Lipid droplets: a unified view of a dynamic organelle. Nat Rev Mol Cell Biol 7:373–378

Maxfield FR, Tabas I (2005) Role of cholesterol and lipid organization in diseases. Nature 438:612–621

Muscatine L (1967) Glycerol excretion by symbiotic algae from corals and Tridacna and its control by the host. Science 156:516–519

Muscatine L, Goiran C, Land L, Jaubert J, Cuif J-P, Allemand D (2005) Stable isotopes (δ^{13} C and δ^{15}N) of organic matrix from coral skeleton. Proc Natl Acad Sci USA 102:1525–1530

Nakamura K, Handa S (1984) Coomassie brilliant blue staining of lipids on thin-layer plates. Anal Biochem 142:406–410

Patton JS, Burris JE (1983) Lipid synthesis and extrusion by freshly isolated zooxanthellae (symbiotic algae). Mar Biol 75:131–136

Peng SE, Luo YJ, Huang HJ, Lee IT, Hou LS, Chen WNU, Fang LS, Chen CS (2008) Isolation of tissue layers in hermatypic corals by

N-acetylcysteine: morphological and proteomic examinations. Coral Reefs 27:133–142

Priscu JC, Priscu LR, Palmisano AC, Sullican CW (1990) Estimation of neutral lipid levels in Antarctic sea ice microalgae by nile red fluorescence. Antarctic Sci 2:149–155

Trench RK (1971) The physiology and biochemistry of zooxanthellae symbiotic with marine coelenterates. III. The effect of homogenates of host tissues on the excretion of photosynthetic products in vitro by zooxanthellae from two marine coelenterates. Proc R Soc Lond B 177:251–264

Turró S, Ingelmo-Torres M, Estanyol JM, Tebar F, Fernández MA, Albor CV, Gaus K, Grewal T, Enrich C, Pol A (2006) Identification and characterization of associated with lipid droplet protein 1: a novel membrane-associated protein that resides on hepatic lipid droplets. Traffic 7:1254–1269

Umlauf E, Csaszar E, Moertelmaier M, Schuetz GJ, Parton RG, Prohaska R (2004) Association of stomatin with lipid bodies. J Biol Chem 279:23699–23709

Veldhuis MJW, Kraay GW, Timmermans KR (2001) Cell death in phytoplankton: correlation between changes in membrane permeability, photosynthetic activity, pigmentation and growth. Eur J Phycol 36:167–177

Venn AA, Loram JE, Douglas AE (2008) Photosynthetic symbioses in animals. J Exp Bot 59:1069–1080

Wang JT, Douglas AE (1997) Nutrients, signals, and photosynthate release by symbiotic algae: the impact of taurine on the dinoflagellate alga *Symbiodinium* from the sea anemone Aiptasia pulchella. Plant Physiol 114:631–636